Modeling of Casting, Welding and Advanced Solidification Processes - XI
Edited by Charles-André Gandin and Michel Bellet
TMS (The Minerals, Metals & Materials Society), 2006

MODELING OF MACROSEGREGATIONS IN DC CASTING OF BRONZE

M. Gruber-Pretzler[1], F. Mayer[1], M. Wu[1], A. Ludwig[1], H. -A. Kuhn[2], J. Riedle[2]

[1]Christian Doppler-Laboratory for Multiphase Modeling of Metallurgical Processes, Department of Metallurgy, University of Leoben, Franz-Josef-Str. 18; Leoben, 8700, Austria
[2]Wieland-Werke AG, Graf-Arco-Straße 36, Ulm, 89079, Germany

Keywords: solidification, macrosegregation, continuous casting, bronze

Abstract

In DC casting (direct chill continuous casting) of Bronze, macrosegregations cause flows in the final product. Besides sedimentation and flotation of equiaxed grains, feeding flow, thermal and solutal buoyancy driven flow, and inlet flow, there are also potential convection mechanisms which influence the formation of macrosegregations. However, the relative importance of these phenomena is difficult to estimate. Since, macrosegregations are formed during solidification processes, where there is relative motion between the melt and the solidifying dendrites their formation is strongly dependent on the flow, especially in the mushy zone. In order to understand the interactions of the different flow phenomena especially in the mush, the influence of the mush permeability on the formation of macrosegregations is investigated. The recent study discusses the impact of different convection types like inlet flow, thermal and solutal buoyancy flow, and feeding flow on macrosegregations in mushy zones with high or low permeabilities. It is shown that low mush permeability results in positive macrosegregations adjacent to the wall, whereas a strong negative segregation is predicted at the centre line. On the other hand, higher permeability causes significant negative macrosegregations at the wall and at the centre line. In addition, the positive macrosegregations between the wall and the centre line are much stronger if a highly permeable mush is considered.

Introduction

In processing metals, solidification is one of the key phenomena. Producers of almost all types of castings are interested to improve the process because defects based on inhomogeneous distributions of alloy elements, cause deterioration of the product. These defects are mainly caused by a large variety of phenomena occurring during solidification. Changes in the solute distribution affection the whole casting are known as macrosegregations. In order to predict these undesired defects, studies have been carried out by many researchers [1-15, 19]. In a recent publication by two of the present authors [16] the columnar-to-equiaxed transition has been modeled with a three-phase volume-averaging approach, where the motion of grains, the melt flow caused by shrinkage and thermo-solutal buoyancy, and the growth of a columnar front were considered.
In the present paper only the columnar solidification part of the above mentioned three-phase approach is used. Therefore, the permeable mushy zone is thought to be composed of cylindrical ‘dendrites’ with a given primary dendrite arm spacing, λ_1. Feeding flow, as well as thermal and solutal buoyancy flow, appears throughout the mushy zone. In a recent publication of the authors [17] four different simulations for a given mush permeability were compared: (i) considering only feeding flow; (ii) considering only thermal buoyancy flow; (iii) considering only solutal buoyancy flow; and (iv) without considering feeding flow and

thermo- solutal convection. In addition, the recent study presents results for the cases (i) to (iv) with a higher mush permeability. Besides two simulations which include all four phenomena simultaneously, one simulation was preformed for each discussed mush permeability.

Model Description and Assumptions

A detailed description of the used equations used is published in [11, 12, 16]. Due to the given page limit, the reader is referred to these references and here just a short outline of the used columnar solidification model used is given.

The model considers two phases, one for the melt and the second for the growing columnar dendrites. For these two phases the conservation equations of mass, species and enthalpy are included. The momentum conservation equation for the melt is solved in addition. The columnar phase is assumed to move with a fixed velocity, namely the casting velocity. The main assumptions of the model used can be summed up as follows:

- The thermodynamics for the binary CuSn system used are calculated by including simplified phase diagram information based on [18]. A constant redistribution coefficient, k, and a constant liquidus slope, m, were used. The solid fraction at the peritectic temperature reaches about 95-98%. Therefore, and because of the fact that the model for the peritectic reaction is still under development, it is assumed that the remaining liquid solidifies over a small temperature interval.
- Nucleation and growth of equiaxed grains are ignored.
- Columnar dendrites are thought to start growing at the mold wall as soon as the temperature drops below liquidus temperature.
- Growing cylinders are used to approximate the columnar dendrites.
- A shell-like growth driven by diffusion around the cylinder is assumed.
- Corresponding source terms to account for feeding flow and thermo-solutal buoyancy driven flow are included.
- Mechanical interaction between the mush and the flow is calculated via Darcy's law

$$\nabla p = f_l \frac{\mu_l}{K} \Delta u \tag{1}$$

  where p is the pressure, f_l is the liquid volume fraction, μ_l is the viscosity of the liquid phase, K is the permeability of the mush and Δu is the velocity difference between the solid and the liquid.
- To model the mush permeability the Blake-Kozeny permeability approach [11, 23] is applied:

$$K = K_0 \frac{f_l^3}{(1 - f_l)^2} \tag{2}$$

  with the empirical factor K_0.

Problem Description

Geometry and Boundary Conditions

For all presented calculations exactly the same geometry and boundary conditions as in [20] are used to allow accurate comparison. For the process simulation a casting velocity of V_{cast}=1.92 mm/s and a casting temperature of T_0 = 1389 K are used. Since the mold is of a cylindrical shape, an axis-symmetrical simulation has been chosen. Fig. 1a schematically shows the mold where (①) indicates the position of the nozzle, (②) shows the free surface on the top, (③) indicates the upper part of the mold which is assumed to be insulating, (④)

shows the lower part of the graphite mold which is surrounded by a copper–steel mold including a water cooling (⑤). Fig. 1b gives an overview of the used boundary conditions. Here (①) gives the position of the inlet, where a pressure inlet is taken. A heat transfer coefficient (HTC) of $h = 50$ W/m²K and a nozzle temperature of $T_{SEN} = 1292$ K are considered for the submerged entry nozzle (SEN) region. For (②), the HTC and the temperature have a value of $h = 50$ W/m²K and $T_{surface} = 325$ K. For (③) almost ideal insulation is assumed where $h = 10$ W/m²K and $T_{mold} = 1292$ K. For (④) $h = 3000$ W/m²K and $T_{mold} = 550$ K and for (⑤) $h = 1000$ W/m²K and $T_{water} = 300$ K. A constant velocity V_{cast} is taken for the outlet (⑥). For the nozzle and for the free surface a slip condition is used. The mold wall is assumed to move with casting velocity. Therefore, a slip condition for the liquid phase and a non-slip condition for the columnar phase are applied. The grid used has a size of 9016 cells and 9296 nodes. As initial conditions, we start with hot melt ($T_{init} = 1292$ K) at rest ($V_{init} = 0$ m/s). The presented results are taken after reaching a steady state.

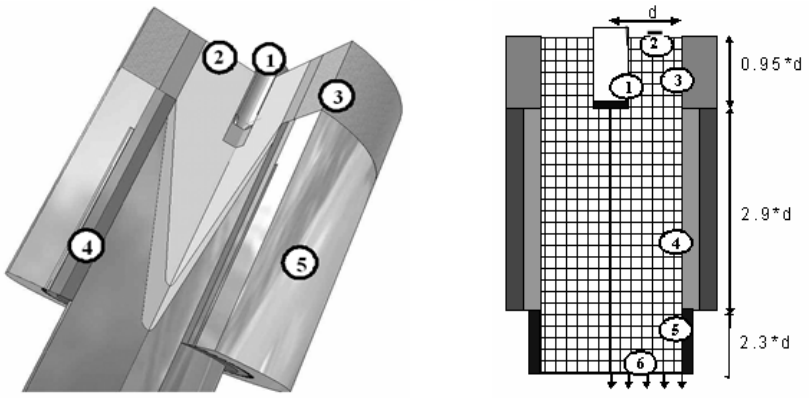

a) b)

Figure 1. (a) Sketch of the considered DC casting process considered: ① nozzle; ② free surface; ③ graphite mold with insulation; ④ graphite and copper mold; ⑤ steel mold with water cooling. (b) Grid and interfaces for boundary conditions (details given in the text).

Case Description

In order to estimate the relative importance of feeding flow, thermal and solutal buoyancy flow, and inlet flow depending on mush permeability, the simulation results from 10 different cases are discussed.

Two different values for the empirical factor in the Blake-Kozeny expression are considered namely i) $K_0 = 2.8 \cdot 10^{-11}$ m^2 and ii) $K_0 = 2.8 \cdot 10^{-9}$ m^2. In addition to the 4 cases studied in [20], one simulation for each K_0 covering all 4 phenomena, is performed. The 5 cases, discussed for both mush permeabilities, can be described as follows:

- Case A: No thermal and solutal buoyancy flow and no feeding flow are considered. We have used equal densities for the liquid and the solid.
- Case B: Here only solutal buoyancy flow is considered. The solutal expansion coefficient has been chosen to be $\beta_c = 0.11\,\text{wt.\%}^{-1}$.
- Case C: Here only thermal buoyancy flow is considered. The thermal expansion coefficient has been chosen to be $\beta_T = 8.6 \cdot 10^{-5}\ \text{K}^{-1}$.
- Case D: For this simulation only feeding flow is considered. We assumed the liquid and solid densities to be independent of temperature and concentration, but different. During solidification the higher solid density then leads to a shrinkage-induced feeding flow.
- Case E: This simulation includes thermal and solutal buoyancy flow in addition to feeding induced flow and forced convection.

To distinguish between low and high permeability calculations, the different cases are labeled with L for low permeability or H for high permeability.

Results and Discussion

To evaluate the influence of the different phenomena on the solidification process, velocity fields and mixed concentrations of the previous mentioned cases are discussed. In all figures the liquidus (T_L = 1289 K), the solidus (T_S = 1230 K) and the temperature where the solidification is thought to be completed (T_P = 1072 K) are shown by isolines. Within the columnar mushy zone, located between T_L and T_P, the volume fraction of the solid varies from 0 to 1. In Fig. 2 the comparison between the velocity fields of the liquid for case B-L and B-H is presented. Fig. 3 shows the velocity fields of the liquid for case C-L and C-H. Fig. 4 and Fig. 5 give a definition of the mixture concentrations:

$$c_{mix} = \frac{c_l . f_l . \rho_l + c_s . f_s . \rho_s}{f_l . \rho_l + f_s . \rho_s} \tag{3}$$

Here, c_l and c_s stand for the concentrations, f_l and f_s stand for the volume fractions and ρ_l and ρ_s for the densities of the liquid and the solid. Fig. 4 shows the cases where $K_0 = 2.8 \cdot 10^{-11}$ m^2 whereas Fig. 5 presents the cases where $K_0 = 2.8 \cdot 10^{-9}$ m^2. As we considered the mush to be permeable, melt-flow occurs through the mush. However, the flow velocities in the mush are much smaller compared to the inlet flow. The incoming melt reveals a velocity as high as V_{in} = 25 mm/s. This large value is a consequence of the constant outlet velocity, V_{cast}, and the overall mass conservation.

The inlet 'jets' hit the mold close to the region where the first solid forms, bend inwards and form corresponding vortices. Due to the assumed K_0, these vortices penetrate into the mushy zone differently for the L and the H cases. Therefore, segregated melt is removed from the mushy zone and replaced by non-segregated 'fresh' melt from the jet vortices. This 'jet-mush' interaction phenomenon takes place in all cases considered (labeled with I in Fig. 4, Fig. 5; all cases). Its strength depends on the velocity of the jet on the one hand and on the permeability of the mush on the other hand. The higher the mush permeability is, the more intensively the jet can meet the mushy zone and wash out an increasing amount of segregated melt. This then results in strong negative surface macrosegregations and more significant positive 'bulk' macrosegregations (Fig. 4, Fig. 5).

In cases A-L and A-H the described 'jet-mush' interaction phenomenon is not overlaid by other phenomena (labeled with I in Fig. 4a, Fig. 5a). The flow from the jet and the flow caused by the withdrawal of the strand are the only convection mechanisms present. However, even in these two cases the negative surface macrosegregations and the positive 'bulk' macrosegregations can be observed with the color scale applied. The comparison shows almost no positive segregation in case A-L but significant ones in case A-H.

In case B-L and B-H, in addition to the inlet jet, solutal buoyancy convection is taken into account (labeled with IIa in Fig. 2b, Fig. 5b). During solidification the liquid in the mushy zone gets enriched with solute and is then forced to rise upwards through the mush (labeled with IIa in Fig. 2b). In case B-L the liquid is not able to move easily between the solidifying dendrites because the low permeability decreases the possibility of convection (Fig. 2a). Also with solute buoyancy, the jet causes negative segregations directly at the wall. In case B-H the high mush permeability enables the enriched liquid to move upwards through the mush untill it impinges on the jet flow. This causes positive macrosegregations at the corresponding position. On the other hand, the solutal buoyancy driven flow from the middle of the strand causes negative centre line segregations.

Thermal buoyancy flow strengthens the inlet jet vortex by the cooled melt flowing down along the solidification front (Fig. 3). As a consequence the 'jet-mush' interaction is increased and more segregated melt is washed out, which in turn leads to more extensive negative surface macrosegregations compared to case A (Fig. 4a and 4c, Fig. 5a and 5c). The washed-out segregated melt is then accumulated by the flow in the middle of the casting, which is the reason for the positive macrosegregations in the 'bulk' of the strand (labeled with II in Fig. 3a and 3b; Fig. 4c, Fig. 5c). The thermal buoyancy driven downwards flow induces an upwards flow in the center of the casting. Thus, melt is carried from deep down

the melt pool upwards, and so the liquidus isoline is shifted up (labeled with III in Fig. 3a and 3b; Fig. 4c, Fig. 5c). This enlarges the mushy zone in comparison with case A. Fig. 3 shows the velocity fields of the upper part of the calculation domains of case C-L (Fig. 3a), and C-H (Fig. 3b) including the "depth of penetration", indicated by broken black lines. The "depth of penetration" is defined as the border between areas where the velocity of the liquid phase is significantly different from that of the solid phase, and when both phases move with almost the same speed and direction, that's when the drag caused by the columnar dendrites dominates. The "depth of penetration" corresponds to about 50% solid fraction for case C-H and 20% solid fraction for case C-L. Due to more free flow through the mushy zone the distribution of the macrosegregations is much more pronounced in case C-H. In the cases considered so far macrosegregations are frozen below the "depth of penetration" (broken black line in Fig. 4c, Fig. 5c).

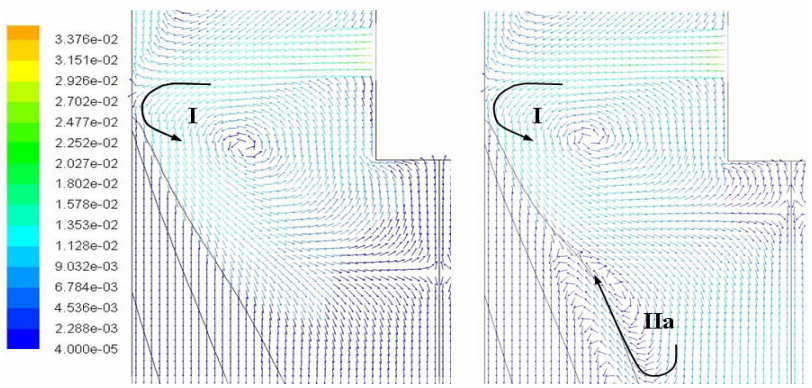

Figure 2: Velocity field at the inlet region (scaled in m/s) (a) for the case with solutal buoyancy flow (case B-L), (b) the same case with the higher permeability (case B-H).

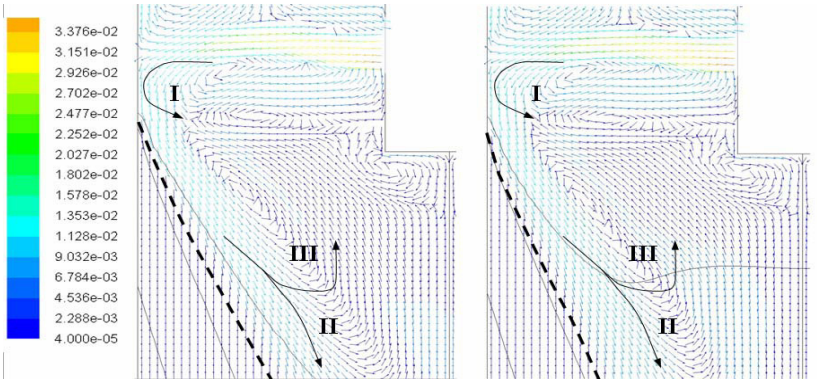

Figure 3: Velocity field at the inlet region (scaled in m/s) (a) for the case with thermal buoyancy flow (case C-L), (b) the same case with the higher permeability (case C-H). Broken black lines indicate the "depth of penetration" (see text).

Up until now, surface macrosegregations are predicted to be negative, and macrosegregations within the casting are predicted to be either negative or positive. However, if shrinkage-induced feeding flow is included and thermo-solutal buoyancy driven flow is ignored, the feature changes. In case D-L the surface macrosegregations turned out to be positive and the macrosegregations in the centre negative (Fig. 5d, see [17]), so just the opposite surface segregation! Feeding flow is always directed from the dendrite tip towards its roots, and thus carries segregated melt into the mush. Since the early work of Flemings in 1967 [21, 22], this phenomenon is known to produce positive macrosegregation at the surface of a casting, the

so-called inverse segregation[1]. This is exactly what happens in case D-L (labeled with IV in Fig. 4d). However, in case D-H the influence of the jet is so high that negative macro-

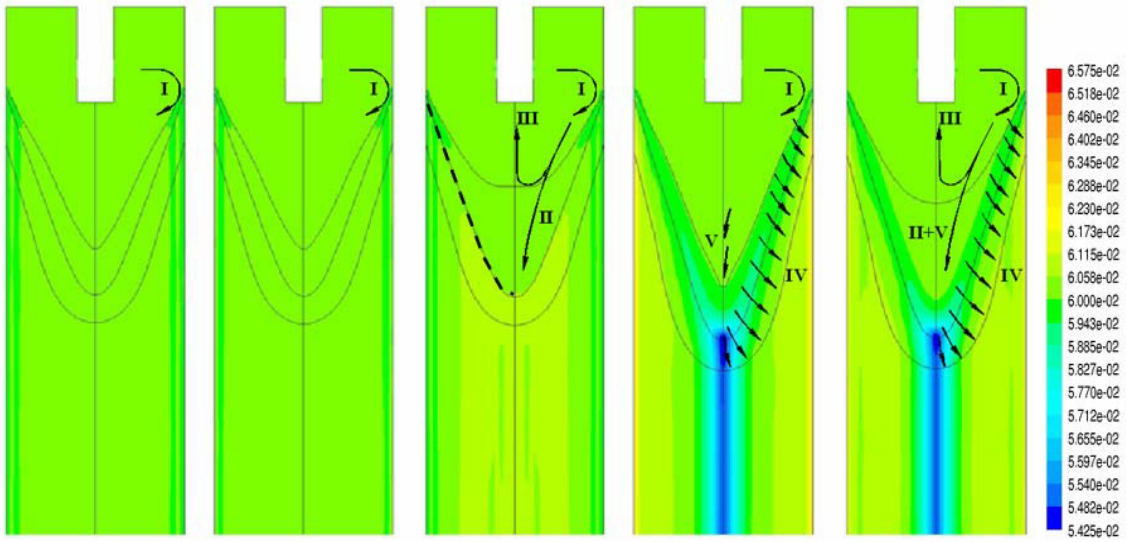

a) b) c) d) e)

Figure 4: Steady-state distributions of the mixture concentration for the five different cases with the lower mush permeability: (a) without feeding and thermo-solutal buoyancy flow (case A-L); (b) only solutal buoyancy flow (case B-L); (c) only thermal buoyancy flow (case C-L) and (d) only feeding flow (case D-L); (e) including feeding and thermo-solutal buoyancy flow (case E-L). Bright green represents the initial alloy concentration, yellow positive and blue negative macrosegregations. Flow patterns are also indicated by arrows.

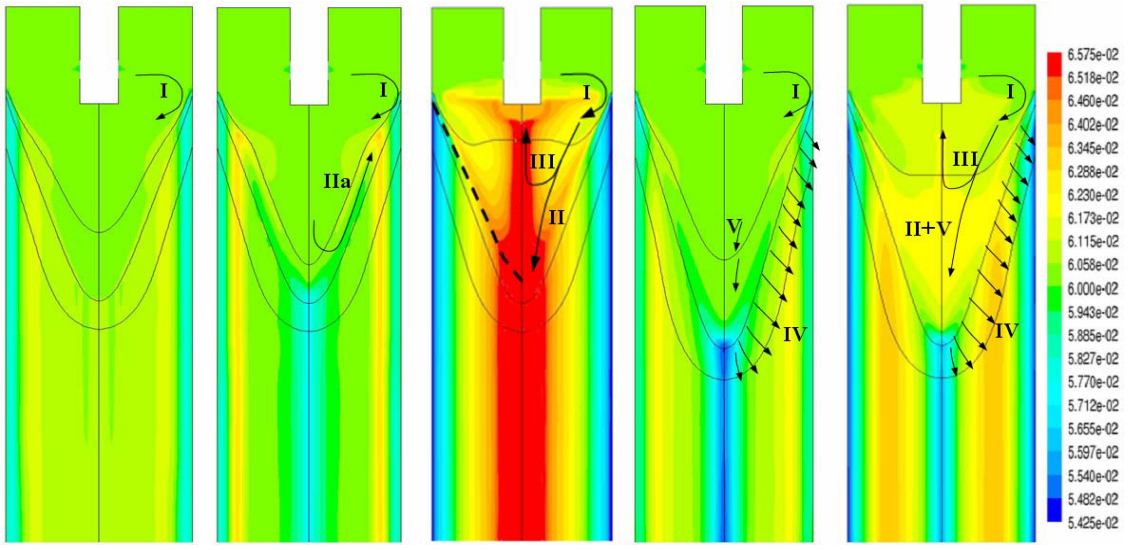

a) b) c) d) e)

Figure 5: Steady-state distributions of the mixture concentration for the 5 cases with the higher mush permeability: (a) without feeding and thermo-solutal buoyancy flow (case A-H); (b) only solutal buoyancy flow (case B-H); (c) only thermal buoyancy flow (case C-H) and (d) only feeding flow (case D-H); (e) including feeding and thermo-solutal buoyancy flow (case E-H). Bright green represents the initial alloy concentration, yellow positive and blue negative macrosegregations. Flow patterns are also indicated by arrows.

segregations still occur at the wall and the positive ones are moved to the adjacent zones (labeled with IV in Fig. 5d). At the centre of the cylindrical casting the dendrite tips approach

[1] Nowadays, inverse (surface) macrosegregation is known to also be caused by an interdendritic flow towards the surface, accompanied by reheating and remelting during the local formation of a gap between the casting and the mold.

each other and form a ring which is going to be closed while solidification proceeds. Besides, a relatively large mush area at the centre is solidifying, and thus a huge amount of melt is needed to feed the corresponding shrinkage. This feeding flow causes the melt to be sucked into the solidifying mush through the closing 'ring of dendrites', and a strong downwards relative velocity occurs in the centre of the casting (labeled with V in Fig. 4d, see ref. [17, 20]). That is why the solidifying dendrites are fed with less- or non-segregated 'fresh' melt from the melt pool, and negative macrosegregations occur in the centre region of the casting. In addition, heat is transferred with the downwards feeding flow, which results in a lower position of the isotherms, especially at the casting centre. In case D-L this phenomena is more pronounced due to the small permeability compared to case D-H. In the latter case, the large K_0 makes feeding through the mush easier. Therefore, the central downwards flow is significantly broader and slower which broadens and decreases the negative centre line segregation (labeled with V in Fig. 5d).

So far, the presented cases give information about the influence of each considered convection phenomena occurring during solidification separately. For the simulations including thermo-solutal buoyancy and feeding flow in addition to the forced convection of the inlet jet, superposition of the different phenomena is expected which indeed can be seen in case E-L and case E-H (Fig. 4e, Fig. 5e). In case E-L positive surface macrosegregations are predicted. Here, the impact of the feeding flow on its formation is decreased by the inlet jet and the thermal buoyancy flow. Directly at the centre line strong negative macrosegregations appear which are caused by the feeding flow but smoothed by the additional effect of thermal convection. Case E-H shows three significant differences compared to case E-L. Firstly, the influence of the inlet jet is so large that negative surface segregations can be observed. Secondly, the positive macrosegregations in the bulk are higher and broader compared to case E-L. This is caused by a strengthening due to thermo-solutal buoyancy flow. Thirdly, the negative centre line macrosegregations are not as pronounced as in case E-L. Here, the strong positive macrosegregations caused by thermal convection (Fig. 5c) are overwhelmed by solutal buoyancy and feeding flow (Fig. 5b, 5d).

Please notice that the predictions presented in this paper depend on the geometry and casting properties considered.

Conclusions

Macrosegregations in DC casting are caused by a relative motion between the solid and the liquid. The present paper investigates how the formation of macrosegregations in DC casting of a columnar solidifying Sn bronze is influenced by the 'inlet jet-mush' interaction, the thermo-solutal buoyancy driven flow and the shrinkage-induced feeding flow, with high and low permeable mushy zones. Conclusions gained from the study of the different macrosegregation formation mechanisms can be gathered as follows:

- For both permeability values used, the 'jet-mush' interaction leads to negative macrosegregations on the surface and positive ones in the bulk of the casting. Here higher permeability leads to more pronounced segregations.
- For the investigated configuration, solutal buoyancy driven flow is negligible in the case of a low permeability. Considering higher permeabilities, negative segregations occur at the wall due to the jet-mush interaction, and in the middle of the casting due to solutal buoyancy. An enrichment of solute is predicted close to the solute-poor region near to the casting wall because solutal buoyancy convection forces the solute-rich fluid to rise through the higher permeable mush.
- For both permeability values used, thermal buoyancy driven flow and its interaction with the inlet jet and the mushy zone plays an important role. The negative surface macrosegregations and the positive bulk macrosegregations are more pronounced in comparison to the case where just inlet flow is considered. For the higher mush permeability, the larger mushy zone enables an increase in macrosegregations throughout the whole casting.

- Shrinkage-induced feeding flow causes macrosegregations at the surface, which are opposite to those which form due to the inlet jet and the thermo-solutal buoyancy driven flow, namely positive ones. In the case with the higher mush permeability the interaction with the jet is stronger than in the case with a lower permeability. Therefore, solute poor solid is formed at the wall, followed by a positive segregated area around negative segregated solid in the centre. In addition, the liquid velocity in the casting centre is reduced, which leads to less negative macrosegregations compared to the case with the lower mush permeability.
- The cases which include feeding flow, thermo-solutal buoyancy flow and forced inlet flow show the expected superposition of the different phenomena. In the case with a lower permeability, positive macrosegregations are predicted at the wall and strong negative ones at the centre line. The higher permeability causes significant changes in the macrosegregation pattern, namely negative segregations at the wall (caused by the inlet jet) and at the centre line (mainly influenced by feeding flow), while for the rest, positive macrosegregations are predicted.

The results show the high dependency of macrosegregations on the flow pattern, and hence on the permeability of the mushy zone. Generally, it can be stated that higher permeability increases the possibility of fluid movement in the mushy zone which goes hand in hand with more pronounced macrosegregations in the casting.
Future studies should also include the nucleation of equiaxed grains which can influence macrosegregations significantly in addition to the flow phenomena discussed.

References

1. M. Rappaz, Int. Mater. Rev. 34, 1989, p. 93.
2. J. Ni, C. Beckermann, Metall. Trans. 22B, 1991, p. 349.
3. C. Beckermann, R. Viskanta, Appl. Mech. Rev. 46, 1993, p. 1.
4. J. Ni, F.P. Incropera, Inter. J. Heat Mass Transfer 38, 1995, p. 1271.
5. J. Ni, F.P. Incropera, Inter. J. Heat Mass Transfer 38, 1995, p. 1285.
6. C.Y. Wang, C. Beckermann, Metall. Mater. Trans. 27A, 1996, p. 2754.
7. C.Y. Wang, C. Beckermann, Metall. Mater. Trans. 27A, 1996, p. 2765.
8. C.Y. Wang, C. Beckermann, Metall. Mater. Trans. 27A, 1996, p. 2784.
9. C. Beckermann, JOM 49, 1997, p. 13.
10. A.V. Reddy, C. Beckermann, Metall. Mater. Trans. 28B, 1997, p. 479.
11. A. Ludwig, M. Wu, Metall. Mater. Trans. 33A, 2002, p. 3673.
12. M. Wu, A. Ludwig, A. Bührig-Polaczek, M. Fehlbier, P.R. Sahm, Inter. J. Heat Mass Transfer 46, 2003, p. 2819.
13. C. Beckermann, C.Y. Wang, Ann. review of heat transfer VI', Vol. 6, pp. 1995, 115-198.
14. P.J.Prescott, F.P. Incropera, Advances in heat transfer, 1996, pp. 231-338.
15. H.Cambeau, B. Appolaire, G. Lesoult, Modeling of casting, welding and advanced solidification processes VIII, 1998, pp. 245-256.
16. M. Wu, A. Ludwig, Metall. Mater. Trans., 2005, in print.
17. M. Gruber-Pretzler, F. Mayer, M. Wu, A. Ludwig. *Continuous Casting*, ed. H.R. Müller (Mannheim, Germany: Wiley-VCH Verlag GmbH&Co. KGaA, 2006), 219-225.
18. T.B. Massalsky, J.L. Murray, L.H. Bennet, H. Baker, Binary Alloy Phase Diagrams, 1986, American Society for Metals, Ohio, Volume 1
19. M.Wu, A. Ludwig, L. Ratke, Modell. Simul. Mater. Sci. Eng. 11, 2003, p. 755.
20. A. Ludwig, M. Gruber-Pretzler, F. Mayer, M. Wu, Mat. Sci. Eng. 2005 in print.
21. M.C. Femings, G.E. Nereo, Trans. Metall. Society AIME 239, 1967, pp. 1449-1460.
22. M.C. Femings, R. Mehrabian, G.E. Nereo, Trans. Metall. Society AIME 242, 1967, pp. 41-49.
23. R.B. Bird, W.E. Steward, E.N. Lightfoot. *Transport Phenomena* (New York, John Wiley & Sons, NY, 1960).